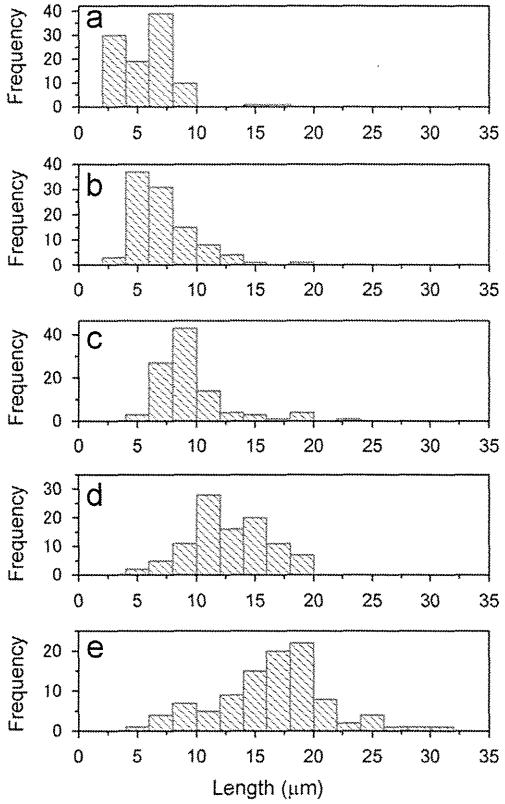

Fig. 3. Length distribution of the C_{60}NWs synthesized using glass bottles with inner diameters of (a) 10 mm, (b) 12.5 mm, (c) 18 mm, (d) 27 mm and (e) 36.5 mm, respectively.

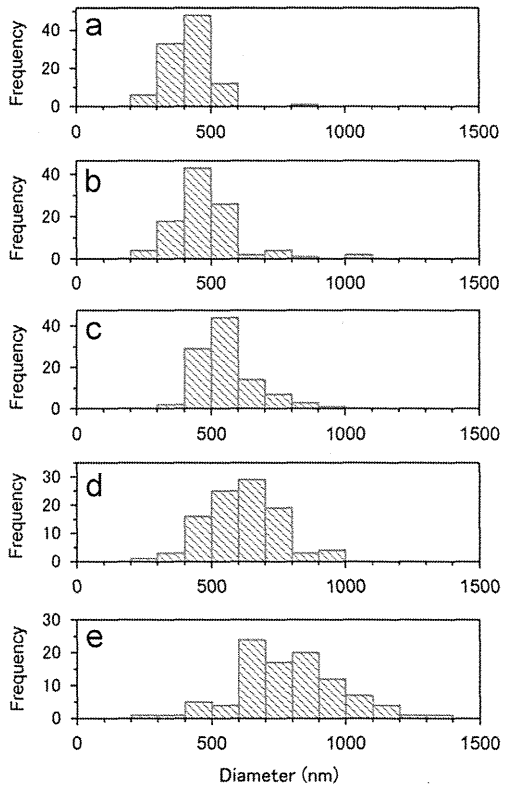

Fig. 4. Diameter distribution of the C_{60}NWs synthesized using glass bottles with inner diameters of (a) 10 mm, (b) 12.5 mm, (c) 18 mm, (d) 27 mm and (e) 36.5 mm, respectively.

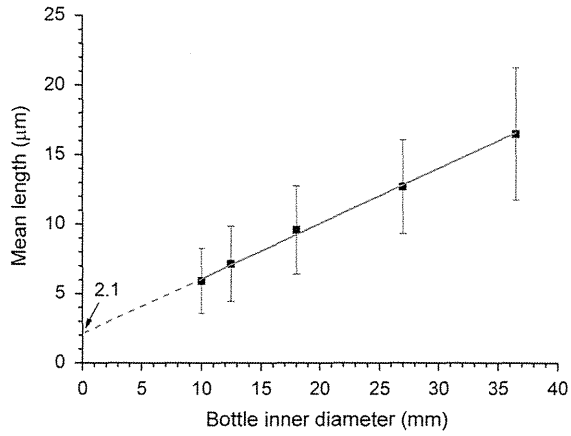

Fig. 5. Mean lengths of the C_{60}NWs (y) plotted relative to the inner diameter of the bottle (x). The fitted curve equation is $y=0.397x+2.1$.

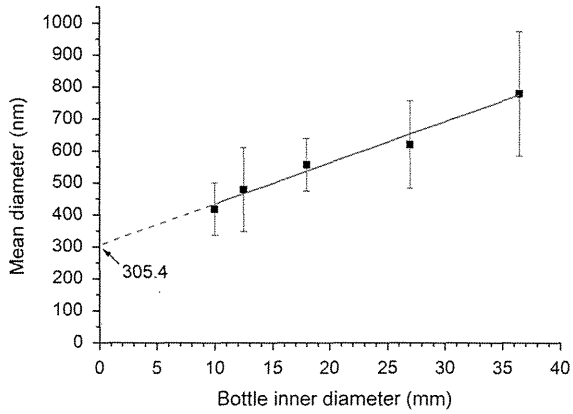

Fig. 6. Mean diameters of the C_{60}NWs (y) plotted relative to the inner diameter of the bottle (x). The fitted curve equation is $y=12.9x+305.4$.

the bottle's inner diameter and were not three-dimensionally performed. Therefore, analyses were also performed using the solution volumes, as shown in Figs. 9–11. The solution volume is defined as the arithmetic sum of the C_{60}-saturated toluene solution and IPA (Table 1).

The length, diameter and aspect ratio of the C_{60}NWs determined from the y-intercepts of Figs. 9–11 are 5.02 μm, 387 nm and 13.1, respectively. The aspect ratio is 5.02 μm/387 nm, producing an aspect ratio of 13.0. Because this value (13.0) is very close to 13.1, the size estimation using the solution volume must be correct. Therefore, the mean size of the C_{60}NW nuclei is estimated to be 5.02 μm long and 387 nm in diameter.

However, the fitted curves in Figs. 9 and 10 show that the mean length and diameter of C_{60}NWs approach the maximum values (16.6 μm and 784 nm, respectively). Therefore, the maximum mean size of the C_{60}NWs attained through the present synthetic method can be estimated from the data obtained after changing the solution volume.

Fig. 12 shows the relationship between the solution volume and the number of C_{60}NWs per unit volume (cm^3) (=number density) formed in the glass bottles. The number of C_{60}NWs in each glass bottle was calculated using the mean size of the C_{60}NWs in the glass bottle and the quantity of C_{60} powder dissolved in the glass bottle when using a saturated solution of C_{60} in toluene (2.58 mg cm^{-3} at 15 °C [21]). The number density of the C_{60}NWs in solution decreases linearly when increasing the solution volume in the double logarithmic plot. The highest number of nuclei per unit volume of solution may be estimated

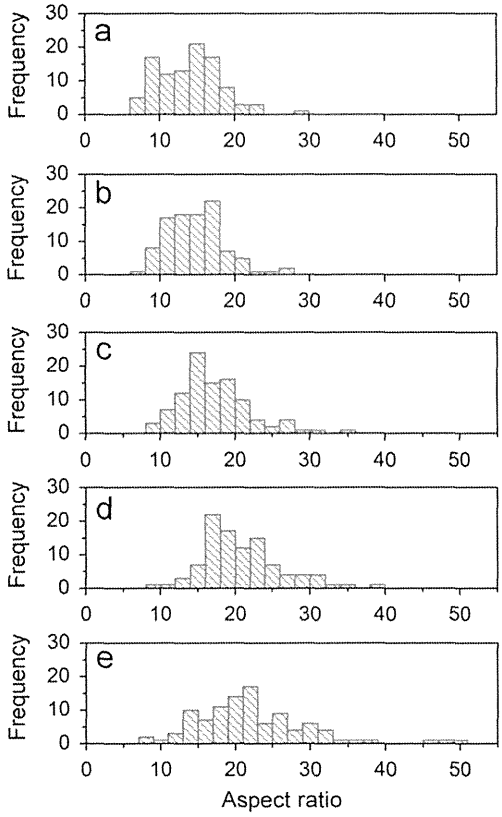

Fig. 7. Aspect ratio distributions of the C_{60}NWs for bottles with inner diameters of (a) 10 mm, (b) 12.5 mm, (c) 18 mm, (d) 27 mm and (e) 36.5 mm, respectively.

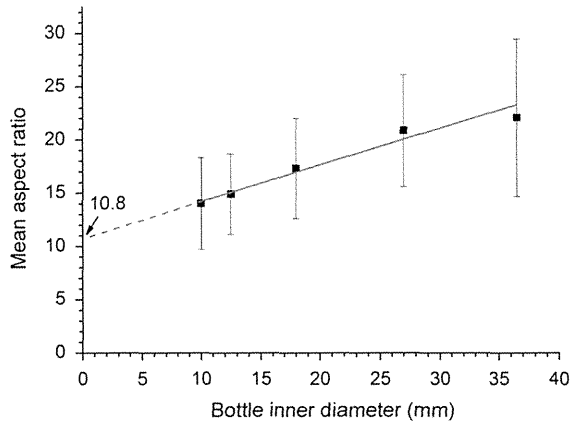

Fig. 8. Relationship between the mean aspect ratio of the C_{60}NWs (y) and the inner diameter of the glass bottles (x). The equation for the fitted curve is $y=0.343x+10.8$.

from the crystal nucleus size calculated for the C_{60}NWs (5.02 μm long and 387 nm in diameter); this value is 1.3×10^9 cm^{-3}. The fitted curve ($y=1.12496\times10^9/x^{0.5674}$) in Fig. 12 shows that the solution volume corresponding to the above number (1.3×10^9 cm^{-3}) is 0.77 cm^3. Therefore, the smallest C_{60}NWs can be obtained when the solution volume is below 0.77 cm^3 and when equal amounts of C_{60}-saturated toluene and IPA are used during the synthetic process.

However, the growth of C_{60}NWs changes depending not only on the solution volume but also on the combination of solvents used in the LLIP method. For example, tubular C_{60}NWs (C_{60} nanotubes) with lengths longer than several millimeters were synthesized, using a LLIP method combined with ultrasonication

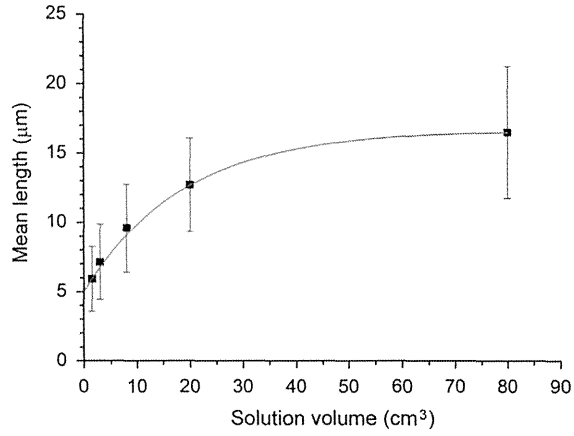

Fig. 9. Relationship between the solution volume (x) and the mean length of the C_{60}NWs (y). The equation for the fitted curve is $y=-11.6\exp(-x/18.7)+16.6$. The mean length asymptotically approaches 16.6 μm.

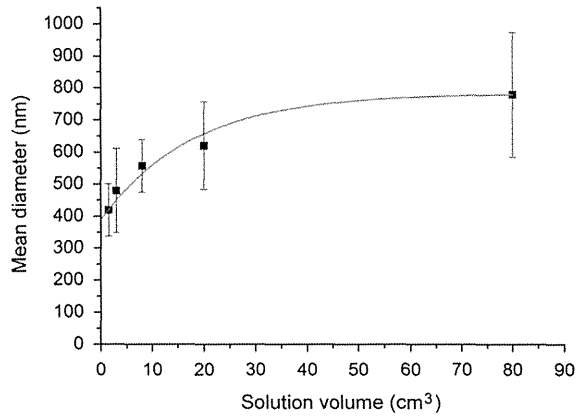

Fig. 10. Relationship between the solution volumes and the mean diameters of C_{60}NWs. The fitted curve equation is $y=-396.6\exp(-x/17.6)+783.7$. The mean diameter approaches 784 nm asymptotically.

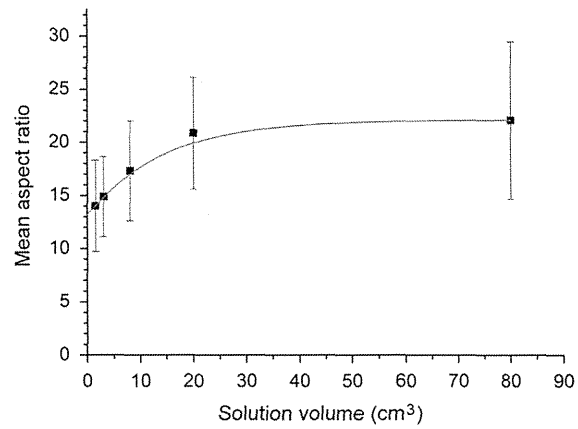

Fig. 11. Relationship between the solution volume (x) and the mean aspect ratio of the C_{60}NWs (y). The equation for the fitted curve is $y=-9\exp(-x/14.2)+22.1$. The mean aspect ratio approaches 22.1 asymptotically.

and manual mixing, where 1 mL of C_{60}-saturated pyridine solution and 9 mL of IPA were used [23]. In this case, although the solution volume was 10 cm^3, the length of C_{60}NWs far exceeds the size of the C_{60}NWs in the present experiment. Thus, in order to elucidate the growth mechanism of C_{60}NWs, how the combination of solvents influences the growth of C_{60}NWs is going to be investigated further.

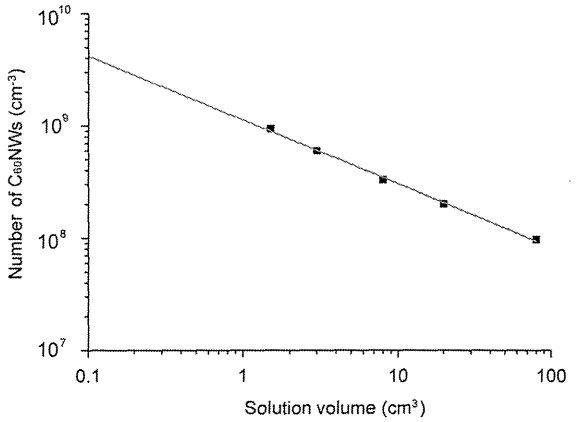

Fig. 12. Estimated number of C_{60}NWs per unit volume plotted versus the solution volume. The equation for the fitted curve is $y=1.12496\times10^{9}/x^{0.5674}$.

4. Conclusions

(1) The mean lengths and diameters of C_{60}NWs increase when increasing the bottle size. However, the size distribution of the C_{60}NWs broadens for the length and diameter when increasing the bottle size.
(2) The mean size of the C_{60}NW crystal nuclei can be determined from the y-intercepts for the mean diameters and lengths of the C_{60}NWs plotted versus the solution volume.
(3) The mean lengths, diameters and aspect ratios for the C_{60}NWs asymptotically approach their upper limits when increasing the solution volume.
(4) The number density of the C_{60}NWs in solution decreases when increasing the solution volume, revealing a linear relationship in their double logarithmic plot.
(5) The minimum size of the C_{60}NWs should be synthesized when the solution volume is below 0.77 cm^3.

Acknowledgments

Portions of this research were supported by the Health and Labor Sciences Research Grant (H24 - Chemistry - Shitei - 009) from the Ministry of Health, Labour and Welfare of Japan, and the JST Strategic Japanese-EU Cooperative Program "Study on managing the potential health and environmental risks of engineered nanomaterials".

References

[1] K. Miyazawa, Y. Kuwasaki, A. Obayashi, M. Kuwabara, J. Mater. Res. 17 (2002) 83.
[2] Fullerene Nanowhiskers, in: K. Miyazawa (Ed.), Pan Stanford Publishing Pte. Ltd., Singapore, 2011.
[3] K. Miyazawa, J. Nanosci. Nanotechnol. 9 (2009) 41.
[4] T. Wakahara, Y. Nemoto, M. Xu, K. Miyazawa, D. Fujita, Carbon 48 (2010) 3359.
[5] L.K. Shrestha, M. Sathish, J.P. Hill, K. Miyazawa, T. Tsuruoka, N.M. Sanchez-Ballester, I. Honma, Q. Ji, K. Ariga, J. Mater. Chem. C 1 (2013) 1174.
[6] L. Wei, J. Yao, H. Fu, ACS Nano 7 (2013) 7573.
[7] J Yang, H. Lim, H.C. Choi, H.S. Shin, Chem. Commun. 46 (2010) 2575.
[8] H. Takeya, K. Miyazawa, R. Kato, T. Wakahara, T. Ozaki, H. Okazaki, T. Yamaguchi, Y. Takano, Molecules 17 (2012) 4851.
[9] H. Takeya, R. Kato, T. Wakahara, K. Miyazawa, T. Yamaguchi, T. Ozaki, H. Okazaki, Y. Takano, Mater. Res. Bull. 48 (2013) 343.
[10] K. Miyazawa, Y. Kuwasaki, K. Hamamoto, S. Nagata, A. Obayashi, M. Kuwabara, Surf. Interface Anal. 35 (2003) 117.
[11] M.P. Larsson, J. Kjelstrup-Hansen, S. Lucyszyn, ECS Trans. 2 (2007) 27.
[12] S.I. Cha, K. Miyazawa, Y.K. Kim, D.Y. Lee, J.-D. Kim, J. Nanosci. Nanotechnol. 11 (2011) 3374.
[13] K. Asaka, R. Kato, K. Miyazawa, T. Kizuka, Appl. Phys. Lett. 89 (2006) 071912.
[14] K. Asaka, R. Kato, R. Yoshizaki, K. Miyazawa, T. Kizuka, Diam. Relat. Mater. 16 (2007) 1936.
[15] K. Saito, K. Miyazawa, T. Kizuka, Jpn. J. Appl. Phys. 48 (2009) 010217.
[16] K. Miyazawa, K. Hotta, J. Cryst. Growth 312 (2010) 2764.
[17] C.L. Ringor, K. Miyazawa, Diam. Relat. Mater. 17 (2008) 529.
[18] M. Tachibana, K. Kobayashi, T. Uchida, K. Kojima, M. Tanimura, K. Miyazawa, Chem. Phys. Lett. 374 (2003) 279.
[19] K. Miyazawa, K. Hotta, J. Nanopart. Res. 13 (2011) 5739.
[20] T. Wakahara, Y. Nemoto, M. Xu, K. Miyazawa, D. Fujita, Carbon 48 (2010) 3359.
[21] K.N. Semenov, N.A. Charykov, V.A. Keskinov, A.K. Piartman, A.A. Blokhin, A.A. Kopyrin, J. Chem. Eng. Data 55 (2010) 13.
[22] K. Hotta, K. Miyazawa, Nano 3 (2008) 355.
[23] K. Miyazawa, C. Ringor, Mater. Lett. 62 (2008) 410.

RESEARCH ARTICLE

Comparative Study of Toxic Effects of Anatase and Rutile Type Nanosized Titanium Dioxide Particles *in vivo* and *in vitro*

Takamasa Numano[1,3], Jiegou Xu[2], Mitsuru Futakuchi[1], Katsumi Fukamachi[1], David B Alexander[2], Fumio Furukawa[3], Jun Kanno[4], Akihiko Hirose[4], Hiroyuki Tsuda[2], Masumi Suzui[1]*

Abstract

Two types of nanosized titanium dioxide, anatase ($anTiO_2$) and rutile ($rnTiO_2$), are widely used in industry, commercial products and biosystems. TiO_2 has been evaluated as a Group 2B carcinogen. Previous reports indicated that $anTiO_2$ is less toxic than $rnTiO_2$, however, under ultraviolet irradiation $anTiO_2$ is more toxic than $rnTiO_2$ *in vitro* because of differences in their crystal structures. In the present study, we compared the *in vivo* and *in vitro* toxic effects induced by $anTiO_2$ and $rnTiO_2$. Female SD rats were treated with 500 μg/ml of $anTiO_2$ or $rnTiO_2$ suspensions by intra-pulmonary spraying 8 times over a two week period. In the lung, treatment with $anTiO_2$ or $rnTiO_2$ increased alveolar macrophage numbers and levels of 8-hydroxydeoxyguanosine (8-OHdG); these increases tended to be lower in the $anTiO_2$ treated group compared to the $rnTiO_2$ treated group. Expression of MIP1α mRNA and protein in lung tissues treated with $anTiO_2$ and $rnTiO_2$ was also significantly up-regulated, with MIP1α mRNA and protein expression significantly lower in the $anTiO_2$ group than in the $rnTiO_2$ group. In cell culture of primary alveolar macrophages (PAM) treated with $anTiO_2$ and $rnTiO_2$, expression of MIP1α mRNA in the PAM and protein in the culture media was significantly higher than in control cultures. Similarly to the *in vivo* results, MIP1α mRNA and protein expression was significantly lower in the $anTiO_2$ treated cultures compared to the $rnTiO_2$ treated cultures. Furthermore, conditioned cell culture media from PAM cultures treated with $anTiO_2$ had less effect on A549 cell proliferation compared to conditioned media from cultures treated with $rnTiO_2$. However, no significant difference was found in the toxicological effects on cell viability of ultra violet irradiated $anTiO_2$ and $rnTiO_2$. In conclusion, our results indicate that $anTiO_2$ is less potent in induction of alveolar macrophage infiltration, 8-OHdG and MIP1α expression in the lung, and growth stimulation of A549 cells *in vitro* than $rnTiO_2$.

Keywords: Nanosized titanium dioxide - anatase - rutile - lung toxicity - MIP1α

Asian Pac J Cancer Prev, **15 (2)**, 929-935

Introduction

There are three mineral forms of natural titanium dioxide particles: rutile, anatase and brookite. Engineered anatase and rutile nanosized titanium dioxide particles ($anTiO_2$ and $rnTiO_2$) are being manufactured in large quantities worldwide and applied in many fields including material industry, electronic industry, commercial products and biosystems. Due to differences in crystal structure, $anTiO_2$ has better photocatalytic activity than $rnTiO_2$ (Kakinoki et al., 2004). Accordingly, $anTiO_2$ is mainly used in paints, such as surface painting of the walls and windows of buildings and vehicles, and photocatalytic systems, while $rnTiO_2$ is preferentially used in cosmetics, sunscreen and food additives.

Large quantity production and widespread application of $nTiO_2$ have given rise to concern about its health and environmental effects. Anatase and rutile type titanium dioxide particles, nanosized and larger, are evaluated as Group 2B carcinogens (possibly carcinogenic to humans) by WHO/International Agency for Research on Cancer (IARC, 2010), based on 2-year animal aerosol inhalation studies (Mohr et al., 2006). Pulmonary exposure to $rnTiO_2$ promotes DHPN-induced lung carcinogenesis in rats, and the promotion effect is possibly associated with $rnTiO_2$ burdened alveolar macrophage derived macrophage inflammatory protein 1 alpha (MIP1α), which acts as a growth factor to stimulate the proliferation of human lung adenocarcinoma cells (A549) *in vitro* (Xu et al., 2010). Dermal application of $anTiO_2$ has been shown to cause significant increases in the level of superoxide dismutase and malondialdehyde in hairless mice (Wu et al., 2009).

Size and photoactivation affect the *in vitro* toxicity of $anTiO_2$ and $rnTiO_2$. $anTiO_2$ (10 and 20 nm) induces

[1]*Department of Molecular Toxicology, Nagoya City University Graduate School of Medical Sciences and Medical School,* [2]*Laboratory of Nanotoxicology Project, Nagoya City University, Nagoya,* [3]*DIMS Institute of Medical Science, Aichi,* [4]*National Institute of Health Sciences, Tokyo, Japan* **For correspondence: suzui@med.nagoya-cu.ac.jp*

oxidative DNA damage, lipid peroxidation and micronuclei formation, and increases hydrogen peroxide and nitric oxide production in BEAS-2B cells, a human bronchial epithelial cell line, but anTiO$_2$ 200 nm particles do not (Gurr et al., 2005). In contrast, both nano-sized and 200nm ruTiO$_2$ are toxic *in vitro* (Gurr et al., 2005; Sayes et al., 2006). On the other hand, under ultraviolet irradiation, anTiO$_2$ is 100 times more toxic to human dermal fibroblasts and A549 cells than rnTiO$_2$, and is more potent than rnTiO$_2$ in the induction of lactate dehydrogenase release, reactive oxygen species production and interleukin 8 secretion (Sayes et al., 2006). Experimental data demonstrating differences in the toxic effects of anTiO$_2$ and rnTiO$_2$ *in vivo*, however, are still lacking.

Respiratory exposure to nTiO$_2$ particles can occur both at the workplace, e.g., in manufacturing and packing sites, and outside the workplace during their use (Maynard et al., 2006; Schulte et al., 2008). In the present study, we delivered anTiO$_2$ and rnTiO$_2$ to the rat lung by trans-tracheal intra-pulmonary spraying (TIPS) and compared lung inflammation and several toxicological parameters induced by anTiO$_2$ and rnTiO$_2$. The results indicated that obvious lung inflammatory lesions were not observed in the rats, and anTiO$_2$ or rnTiO$_2$ particles were phagocytosed by alveolar macrophages. Analysis of alveolar macrophage induction, 8-OHdG level in the lung, and MIP1α expression both *in vivo* in the lung and *in vitro* in PAM indicated that anTiO$_2$ elicited lower levels of biological responses than rnTiO$_2$. Long-term toxic effects of anTiO$_2$ and rnTiO$_2$ still need to be clarified.

Materials and Methods

Preparation and characterization of nTiO$_2$ suspension

Nanosized TiO$_2$ particles (anatase type without coating, primary size 25 nm and rutile type without coating, primary size 20 nm) were provided by Japan Cosmetic Association, Tokyo, Japan. Both anTiO$_2$ and rnTiO$_2$ particles were suspended in saline at 500 μg/ml and then autoclaved. The suspensions were sonicated for 20 min shortly before use to prevent aggregate formation.

Characterization of nTiO$_2$ was conducted as follows: The shapes of nTiO$_2$ in suspension were imaged by transmission electron microscopy (TEM) and scanning electron microscopy (SEM). Element analysis was performed by a an X-ray microanalyzer (EDAX, Tokyo, Japan), after aliquots of nTiO$_2$ were loaded onto a carbon sheet. For size distribution analysis, aliquots of the 500 μg/ml nTiO$_2$ suspension were loaded onto clean glass slides and photographed under a polarized light microscope (Olympus BX51N-31P-O polarized light microscope, Tokyo, Japan), and the photos were then analyzed by an image analyzer system (IPAP, Sumika Technos Corporation, Osaka, Japan). Over 1000 particles of anTiO$_2$ and rnTiO$_2$ were measured.

Animals

Female Sprague-Dawley rats (SD rats) were purchased from CLEA Japan Co., Ltd (Tokyo, Japan). The animals were housed in the animal center of Nagoya City University Medical School, maintained on a 12 hour light-dark cycle and received oriental MF basal diet (Oriental Yeast Co., Tokyo, Japan) and water *ad lib*. The research was conducted according to the Guidelines for the Care and Use of Laboratory Animals of Nagoya City University Medical School and the experimental protocol was approved by the Institutional Animal Care and Use Committee (H22M-19).

Trans-tracheal intra-pulmonary spraying (TIPS) protocol

Three groups of 6 female SD rats (Group 1, saline; Group 2, anTiO$_2$; and Group 3, rnTiO$_2$) aged 9 weeks were acclimated for 7 days prior to the start of the study. Saline and nTiO$_2$ suspensions were administered by TIPS to the animals under isoflurane anesthesia: The nozzle of a Microsprayer (series IA-1B Intratracheal Aerosolizer, Penn-century, Philadelphia, PA) connected to a 1 ml syringe was inserted into the trachea through the larynx and a total volume of 0.5 ml suspension was sprayed into the lungs synchronizing with spontaneous inspiration by the animal (Xu et al., 2010). Rats were treated once every the other day over a 2 week period, a total of eight treatments. The total amount of anTiO$_2$and rnTiO$_2$ administered to Groups 2 and 3 was 2.0 mg per rat. Six hours after the last spraying, the animals were killed and the whole lung was excised and divided into two parts; the left lung was cut into pieces and immediately frozen at -80°C and used for biochemical analysis, and the right lung was fixed in 4% paraformaldehyde solution in phosphate-buffered saline (PBS) adjusted to pH 7.3 and processed for immunohistochemical, light microscopic and transmission electron microscopic (TEM) examinations.

Light microscopy and transmission electron microscopy

Hematoxylin and eosin (H&E) stained sections were used for pathological observation. The number of alveolar macrophages in H&E lung tissue slides was counted and expressed as number per mm^2.

Slides were observed under light microscopic observation, the corresponding area in the paraffin block was cut out, deparaffinized and embedded in epoxy resin and processed for TEM and titanium element analysis with a JEM-1010 transmission electron microscope (JEOL Co. Ltd, Tokyo, Japan) equipped with an X-ray microanalyzer (EDAX, Tokyo, Japan).

Analysis of 8-hydroxydeoxy guanosine levels

For the analysis of 8-hydroxydeoxyguanosine (8-OHdG) levels, genomic DNA was isolated from a piece of the left lung with a DNA Extractor WB kit (Wako Chemicals Co. Ltd). 8-OHdG levels were determined with an 8-OHdG ELISA Check kit (Japan Institute for Control of Aging, Shizuoka, Japan).

RNA isolation, cDNA synthesis and RT-PCR analysis of gene expression

Pieces of the left lungs (50-100 mg) were thawed, rinsed 3 times with ice cold PBS, and total RNA was isolated using 1 ml Trizol Reagent (Invitrogen, Karlsruhe, Germany). For reverse transcription PCR (RT-PCR) and real-time PCR, first strand cDNA synthesis from 2 mg of total RNA was performed using SuperScript™ III First-Strand Synthesis

System (Invitrogen of Life Technologies, CA) according to the manufacturer's instructions. PCR primers for rat MIP1α were 5'-TTTTGAGACCAGCAGCCTTT -3' (forward) and 5'- CTCAAGCCCCTGCTCTACAC-3' (reverse), and the product size was 191bp. b-actin was used as internal control and the primers were 5'- AGCCATGTACGTAGCCATCC-3' (forward) and 5'-CTCTCAGCTGTGGTGGTGAA-3', and the product size was 228 bp. RT-PCR was conducted using an iCycler (BioRad Life Sciences, CA) as follows: 95°C 20 sec, 60°C 20 sec, 72°C 30sec, 30 cycles for MIP1α; and 95°C 20 sec, 60°C 20 sec, 72°C 30sec, 15 cycles for b-actin. Real-time PCR analysis of MIP1α gene expression was performed with a 7300 Real Time PCR System (Applied Biosystem, CA) using Power SYBR Green PCR Master Mix (Applied Biosystem, CA) according to the manufacturer's instructions. b-actin gene was used as the normalizing reference gene.

Immunohistochemical analysis

Paraffin embedded lung tissues sections were immunostained with polyclonal anti-rat MIP1α (BioVision, Lyon, France). Antigen retrieval was carried out by microwave for 20 min in 10 mmol/L citrate buffer (pH 6.0). Antibody was diluted 1:100 in blocking solution and applied to the slides, and the slides were incubated at 4°C overnight. Immunohistochemical staining was done by the avidin-biotin complex method (ABC) using the Vectastain Elite ABC system (Vector Laboratories, Burlingame, CA). Biotinylated goat anti-rabbit IgG (Vector Laboratories) was used as a secondary antibody at a dilution of 1:500 for 1 hour and visualized using avidin-conjugated alkaline phosphatase complex (ABC kit, Vector laboratories) and Alkaline Phosphatase Substrate Kit (Vector Laboratories). Sections were lightly counterstained with hematoxylin for microscopic examination.

ELISA for MIP1α in the lung tissues and the supernatants of cell culture

Left lung tissue samples (50-100mg) were thawed, rinsed 3 times with ice cold PBS and homogenized in 1 ml of tissue extraction reagent (PeproTech, London, UK) containing 1% (v/v) Proteinase Inhibitor Cocktail (Sigma-Aldrich, St Louis, MO, USA). The homogenates were clarified by centrifugation at 10,000g, 4°C for 5 min. The protein content in the supernatants was measured with a BCATM Protein assay kit (Pierce). The levels of MIP1α in the supernatants were measured using rat MIP1α ELISA Development Kit (Cat#: 900-K75, Peprotech, Inc., Rocky Hill, NJ.) according to the manufacturer's instruction, and expressed as pg/mg lung tissue protein. The levels of MIP1α in cell culture supernatants were measured as described above and expressed as pg/ml.

Isolation of PAM and exposure of $nTiO_2$ to PAM cells

Induction and isolation of alveolar macrophages in female SD rats was performed as described previously (Xu et al., 2010). 10^6 primary alveolar macrophages (PAM) were cultured in RPMI1640 containing 2% fetal bovine serum and antibiotics overnight at 37°C, 5% CO_2. 500 μg/ml of $anTiO_2$ and $rnTiO_2$ suspensions was then added to the cultures to a final concentration of 10 μg/ml and the cells were incubated for another 24 hours. RNA was isolated from the PAM and the level of MIP1α protein in the conditioned culture media was measured by ELISA.

In vitro cell proliferation assay

A549 cells were seeded into 96-well culture plates at 2×10^3 cells per well in 2% fetal bovine serum Dulbecco's modified Eagle's medium (Wako Chemicals Co., Ltd). After overnight incubation, the medium was replaced with the conditioned PAM culture media treated with $anTiO_2$ or $rnTiO_2$, and the cells were incubated for another 72 hours, with or without 20 μg/ml of anti-MIP1α neutralizing antibody (R&D Systems, Minneapolis, MN). The relative cell number of A549 cells was determined using a Cell counting Kit-8 (Dojindo Molecular Technologies, Rockville, MD) according to the manufacturer's instruction.

Cytotoxicity assay in vitro

A549 cells, the primary human lung fibroblast cell line CCD34 (ECACC, Cat. No. 90110514) and PAM were used for cytotoxicity analyses. Cells were seeded in 96 well plates at 5×10^3/well and incubated overnight. The cells were then treated with $anTiO_2$ and $rnTiO_2$ suspensions at final concentrations of 0, 2, 10, or 50 μg/ml and then incubated for another 24 hours. The relative cell number was determined as described above.

Cytotoxicity of $anTiO_2$ and $rnTiO_2$ under ultraviolet B irradiation

A549 cells were used for analysis of $nTiO_2$ cytotoxicity under ultraviolet irradiation. First, we determined an irradiation time that did not affect the cell viability as follows: A549 cells were seeded into 96 well plates at 1×10^3/well in 200 μL Dulbecco's modified Eagle's medium (Wako Chemicals Co., Ltd) containing 10% fetal bovine serum and incubated overnight. The cells were irradiated with ultraviolet B (UVB) for 0, 30 sec, 1 min, 2 min, 5 min and 10 min with a transilluminator (Vilber Lourmat, France). The light intensity was 1000 mW/cm^2, and the emission spectrum was from 270 nm to 330 nm with a peak at 312 nm. The non-irradiated control wells were covered with a sterile aluminium sheet to prevent irradiation. The relative cell number was determined after incubation for 48 hours at 37°C, 5% CO_2.

Next, we observed the effect of $anTiO_2$ and $rnTiO_2$ on cell viability under UVB. A549 cells were seeded into 96 well plate at 1×10^3well in 100 μL culture media and incubated overnight. Then, 100 mL of $anTiO_2$ or $rnTiO_2$ suspensions in DMEM culture medium containing 10% FBS was added into the wells to final concentration of 0, 2, 5 and 10 μg/ml and incubated for 30 min. The cells were irradiated with UVB for 2 min (2 min UVB irradiation did not affect cell viability), and incubated for another 48 hours, before determination of relative cell number.

Statistical and analysis

Statistical significance of the *in vitro* and *in vivo* findings was analyzed using the two-tailed Student's t-test. *In vitro* and *in vivo* data are presented as means±standard

deviations. A value of $p<0.05$ was considered to be significant.

Results

Characterization of $nTiO_2$ particles in suspension

TEM images showed that individual $anTiO_2$ particles were spherical in shape, while individual $rnTiO_2$ particles had a rod-like shape, and both $anTiO_2$ and $rnTiO_2$ formed large aggregates in suspension (Figure. 1A and B). Similarly, SEM observation indicated aggregate formation of both types of $nTiO_2$ particles (Figure. 1C and D). Peaks of titanium (green arrows) and oxygen (blue arrows), which are present in both types of $nTiO_2$ particles, and carbon (white arrows) and nitrogen (red arrow), which are present in the carbon sheets used in the SEM, were observed by elemental scanning (Figure. 1E and F). Peaks of other elements were not detected in either the $rnTiO_2$ or $anTiO_2$ samples. Analyses of particle size showed that the mean and medium diameters were 5.491±2.727 mm and 5.127 mm for $anTiO_2$, and 3.799±2.231 mm and 3.491 mm for $rnTiO_2$ (Figure. 1G), confirming aggregate formation of both types of $nTiO_2$ particles in suspension.

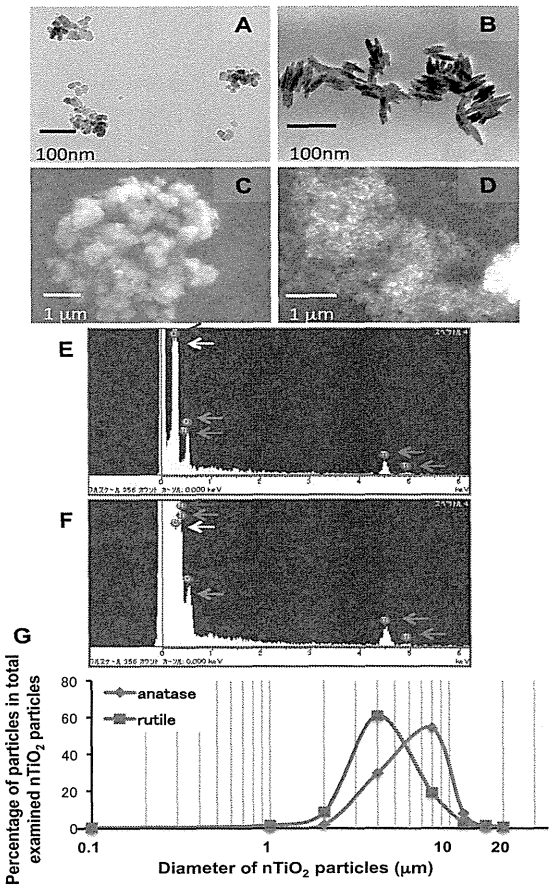

Figure 1. Characterization of $nTiO_2$ Particles in Suspension. A and B: TEM imagines of $anTiO_2$ and $rnTiO_2$ particles in suspension. C and D: SEM images of $anTiO_2$ and $rnTiO_2$ particles. E and F: Element scanning showed peaks of titanium (green arrows), oxygen (blue arrows), carbon (white arrows) and nitrogen (red arrows) in $anTiO_2$ and $rnTiO_2$ particles. G: Size distribution of $anTiO_2$ and $rnTiO_2$ in suspension

Histological observation and 8-OHdG level in the lung tissue

Only a few small lung inflammatory lesions were observed in rats treated with $anTiO_2$ and $rnTiO_2$ (Figure. 2A, B and C). Alveolar macrophage infiltration was found throughout the lung tissue, and most of the alveolar macrophages were seen with phagocytosed $anTiO_2$ particles or $rnTiO_2$ particles (Figure. 2D, E an F). TEM observation demonstrated that both $anTiO_2$ and $rnTiO_2$ were deposited in various sizes in the cytoplasm of the alveolar macrophages (Figure. 2G and H). Neither $anTiO_2$ or $rnTiO_2$ particles were found in other types of cells in the lung tissue. The number of macrophages per mm^2 lung tissue section was 67.1±15.8 (saline), 165.0±34.9 ($anTiO_2$) and 214.2±44.1 ($rnTiO_2$). The numbers of macrophages in the $anTiO_2$ and $rnTiO_2$ treated groups was significantly higher than in the control group ($p<0.001$), and the $anTiO_2$ treated group had lower macrophage infiltration than the $rnTiO_2$ treated group.

The level of 8-OHdG, a parameter of oxidative DNA damage caused by reactive oxygen species (ROS), in the lung tissue in rats treated with $anTiO_2$ and $rnTiO_2$ was 1.96±0.77 and 3.07±1.25 (pg per mg DNA), respectively, and was higher than that of the control (1.44±0.63): The increase in 8-OHdG in the lungs of $rnTiO_2$, but not $anTiO_2$, treated rats was significantly higher than the control

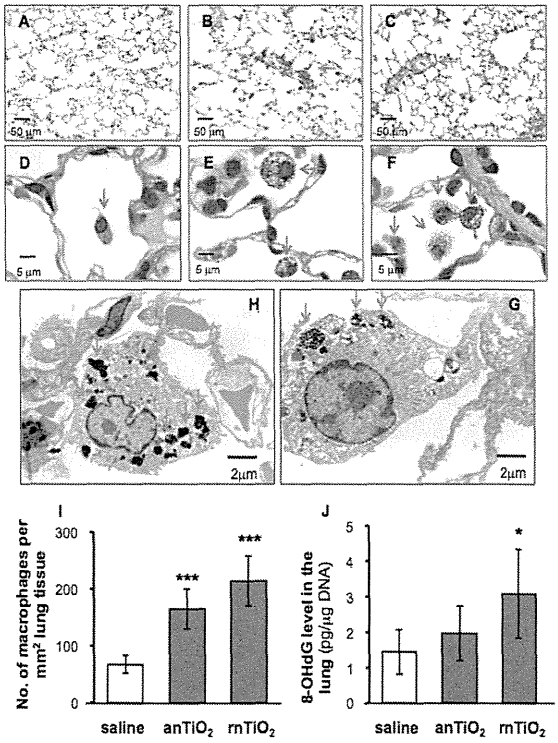

Figure 2. Histological Observation and 8-OHdG Level in the Lung Tissue. A, B and C: Histological imagines of lung tissue treated with saline, $anTiO_2$ and $rnTiO_2$, respectively. Green arrows indicate small inflammatory lesions. D (saline), E ($anTiO_2$) and F ($rnTiO_2$): Higher magnification imagines of alveolar macrophages (brown arrows). $nTiO_2$ particles are clearly observed. G and H: TEM imagines of alveolar macrophages with $anTiO_2$ and $rnTiO_2$ particles in their cytoplasm (blue arrows). I and J: The numbers of alveolar macrophages and 8-OHdG levels in the lung tissue. *, *** represent $p<0.05$ and 0.001, respectively, versus saline

($p<0.05$) (Figure. 2J).

MIP1α expression in the lung tissue

RT-PCR suggested an increase in MIP1α mRNA expression in lung tissue treated with $anTiO_2$ or $rnTiO_2$ (Figure. 3A). Real-time PCR analysis indicated that compared with the control group, the increase was 2.79-fold for $anTiO_2$ and 5.35-fold for $rnTiO_2$. MIP1α mRNA expression was also significantly lower in the $anTiO_2$ treated group compared to the $rnTiO_2$ treated group (Figure. 3B). The levels of MIP1α protein in the lung tissue were 32.8±0.31 and 52.7±0.58 pg/mg lung protein in the $anTiO_2$ and $rnTiO_2$ treated groups, both significantly higher than that of the control group (20.8±0.24) (Figure. 3C). Similarly to MIP1α mRNA expression, MIP1α protein expression was significantly lower in the $anTiO_2$ treated group compared to the $rnTiO_2$ treated group.

To find out what cells in the lung accounted for the increased MIP1α protein expression, we examined tissue samples using MIP1α immunohistochemistry. As shown in Figure. 3D, E and F, MIP1α protein was produced by $anTiO_2$ or $anTiO_2$ burdened alveolar macrophages.

Exposure of PAMs to $anTiO_2$ and $rnTiO_2$ and cell proliferation assays in vitro

As in the lung tissue, *in vitro* exposure of PAM to $nTiO_2$ induced expression of MIP1α mRNA (Figure. 4A) and protein (Figure. 4B). Treatment with $anTiO_2$ and $rnTiO_2$ caused 11.96-fold and 15.26-fold increases in the expression of MIP1α mRNA, respectively, in cultured PAM. The level of MIP1α protein in the cell culture medium was 32.8±1.1 pg/mL for $anTiO_2$ and 52.7±1.3 pg/mL for $rnTiO_2$, significantly higher than that of the control (20.8±1.2 pg/mL). Both mRNA and protein expression of MIP1α was significantly lower in the $anTiO_2$ treated PAM compared to the $rnTiO_2$ treated cells.

The supernatants of the culture media of PAM treated with $anTiO_2$ showed only a tendency to increase A549 cell proliferation, while those collected from PAM treated with $rnTiO_2$ significantly promoted proliferation of A549 cells (115%) compared to supernatants from the saline treated group (Figure. 4C). The promotion effect of the supernatants of PAM cell cultures treated with $anTiO_2$or

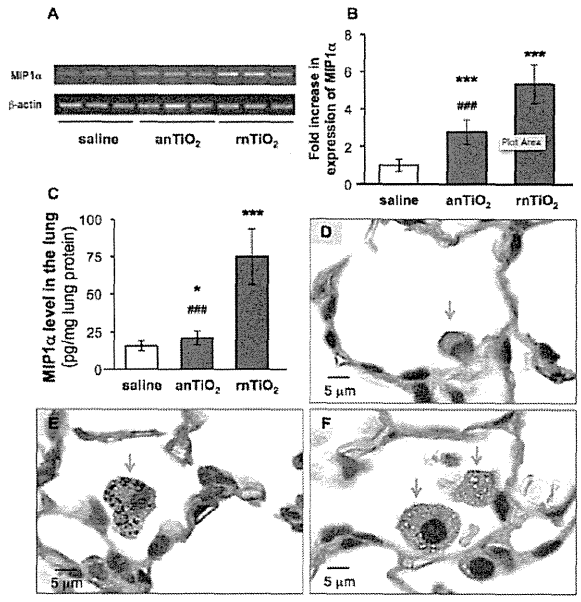

Figure 3. Expression of MIP1α in the Lung Tissue. A, B and C: Analysis of expression of MIP1α mRNA by RT-PCR (A) and real-time PCR (B) and protein by ELISA (C). D, E, and F: Immunohistochemistry shows MIP1α expressed in alveolar macrophages of lung tissue treated with saline (D), $anTiO_2$ (E) and $rnTiO_2$ (F). *, *** represent $p<0.05$ and 0.001, respectively, versus saline; ### represent $p<0.001$, versus $rnTiO_2$

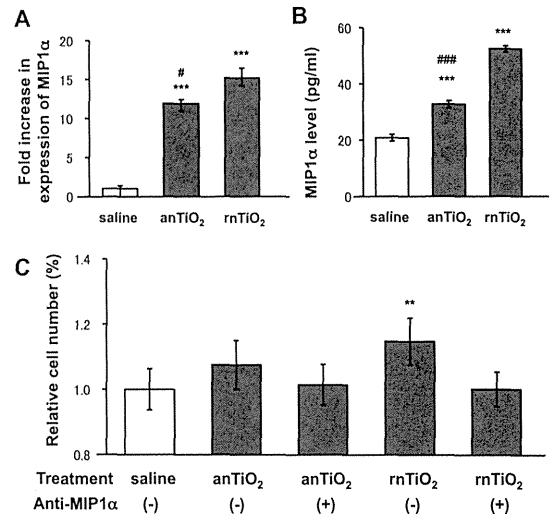

Figure 4. The Effect of $anTiO_2$ and $rnTiO_2$ on PAM Cells. The expression of MIP1α mRNA in cultured PAM (A) and protein in the culture media (B) indicate that treatment with $anTiO_2$ or $rnTiO_2$ increased MIP1α expression in the PAM. Conditioned cell culture media of PAM treated with $rnTiO_2$, but not $anTiO_2$, had a significant effect on proliferation of A549 cells, and this promotion was attenuated by addition of 20 μg/ml MIP1α neutralizing antibody (C). **, ***represent $p<0.01$ and 0.001, versus saline; #, ###represent $p<0.05$ and 0.001, versus $rnTiO_2$

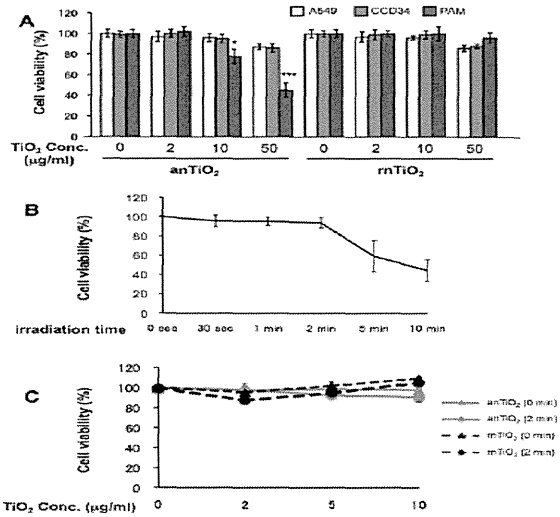

Figure 5. *In vitro* Assays. A: The effect of $anTiO_2$ and $rnTiO_2$ on the viability of A549, CCD34 and PAM cells. B: The effect of UVB irradiation on the viability of A549 cells. C: The effect of $anTiO_2$ and $rnTiO_2$ on the vi ability of A549 under UVB irradiation. *, *** represent $p<0.05$ and 0.001, versus the vehicle

$rnTiO_2$ was attenuated by anti-MIP1α neutralizing antibodies, indicating MIP1α is probably a mediator of the increase in A549 cell proliferation.

In vitro cytotoxicity assays

In vitro cytotoxicity assays indicated that both $anTiO_2$ and $rnTiO_2$ had little effect on the cell viability of A549 and CCD34 cells at a concentration of up to 50 mg/ml. $anTiO_2$ had a cytotoxic effect on the cell viability of PAM at doses of 10 and 50 mg/ml, while $rnTiO_2$ did not impair the cell viability of PAM at any of the examined concentrations (Figure. 5A).

To investigate whether UVB irradiation affected the cytotoxic effects of $anTiO_2$ and $rnTiO_2$ on cell viability, we first determined the exposure times that ultraviolet B irradiation itself did not impair the viability of A549 cells. As shown in Figure. 5B, irradiation for up to 2 min did not have any effect on the viability of A549 cells. With 2 min of UVB irradiation, neither $anTiO_2$ or $rnTiO_2$ at doses of 2, 5 or 10 μg/ml resulted in any decrease in the viability of A549 cells (Figure. 5C).

Discussion

The toxicity of nanoparticles usually includes tiers of biological responses such as induction of ROS and inflammation (Nel et al., 2006). This may contribute to carcinogenic potential (Tsuda et al., 2009). Thus, in the present study, we compared several parameters ofr inflammation and oxidative stress induced by TIPS of $anTiO_2$ and $rnTiO_2$. The results indicated that both $anTiO_2$ and $rnTiO_2$ particles were phagocytosed by alveolar macrophages and did not cause strong lung inflammation. Treatment with $anTiO_2$ and $rnTiO_2$ increased alveolar macrophage infiltration, MIP1α expression and 8-OHdG production: $anTiO_2$ had less effect than $rnTiO_2$.

Phagocytosis by alveolar macrophages is a major defense mechanism for deposition and clearance of inhaled particles (Heppleston, 1984; Rom et al., 1991; Geiser et al., 2008). However, activation of alveolar macrophages is strongly associated with inflammatory reactions and ROS production (Renwick et al., 2001; Bhatt et al., 2002; Wang et al., 2007). Also, MIP1α, secreted from $rnTiO_2$ burden alveolar macrophages, is possibly involved in the promotion of lung carcinogenesis (Xu et al., 2010). Similarly, pleural macrophage recruitment and activation are involved in the pathogenesis of asbestos (Choe et al., 1997). These results indicate two contrasting roles of alveolar macrophages in pathogenesis and host defense.

The toxic effects of nanoparticles are dependent on their size, shape, surface functionality and composition (Albanese et al., 2012). In the present study, we used comparable sizes of $anTiO_2$ and $rnTiO_2$ particles. Both types of $nTiO_2$ had no surface coating and had no obvious difference in elemental composition. Therefore, differences in alveolar macrophage induction, MIP1α expression and 8-OHdG production between $anTiO_2$ and $rnTiO_2$ are likely due to their different crystal structures and shapes. The lower toxicity of $anTiO_2$ compared to $rnTiO_2$ in the absence of UVB irradiation in our study is consistent with a previous *in vitro* study with bulk rutile and anatase TiO_2 (Gurr et al., 2005). In contrast to a previous study (Sayes et al., 2006), in the present study $anTiO_2$ and $rnTiO_2$ did not exhibit different toxicities on the cell viability of A549 cells under ultraviolet irradiation.

It should be noted that both types of $anTiO_2$ and $rnTiO_2$ particles formed aggregates in suspension, and aggregation may alter their bio-reactivity. Whether $anTiO_2$ and $rnTiO_2$ particles have different long-term effects remains to be clarified.

In conclusion, *in vivo* exposure of the rat lung to $anTiO_2$ or $rnTiO_2$ particles increased alveolar macrophage infiltration, MIP1α expression and 8-OHdG production, with $anTiO_2$ eliciting lower levels of biological responses than $rnTiO_2$. Similarly, exposure of primary alveolar macrophages to $rnTiO_2$ *in vitro* resulted the cells producing more MIP1α mRNA and protein than cells exposed to $anTiO_2$. Cytotoxicity assays *in vitro* indicated that both $anTiO_2$ and $rnTiO_2$ had very low cellular toxicity even under UVB irradiation.

Acknowledgements

This work was supported by Health and Labour Sciences Research Grants (Research on Risk of Chemical substance, H19-kagaku-ippan-006 and H22-kagaku-ippan-005). We thank Chisato Ukai and Takako Narita for their excellent secretarial assistance for the work.

References

Albanese A, Tang PS, Chan WC (2012). The effect of nanoparticle size, shape, and surface chemistry on biological systems. *Annu Rev Biomed Eng*, **14**, 1-16.

Bhatt NY, Kelley TW, Khramtsov VV, et al (2002). Macrophage-colony-stimulating factor-induced activation of extracellular-regulated kinase involves phosphatidylinositol 3-kinase and reactive oxygen species in human monocytes. *J Immunol*, **169**, 6427-34.

Choe N, Tanaka S, Xia W, et al (1997). Pleural macrophage recruitment and activation in asbestos-induced pleural injury. *Environ Health Perspect*, *105*, 1257-60.

Geiser M, Casaulta M, Kupferschmid B, et al (2008). The role of macrophages in the clearance of inhaled ultrafine titanium dioxide particles. *Am J Respir Cell Mol Biol*, **38**, 371-6.

Gurr JR, Wang AS, Chen CH, et al (2005). Ultrafine titanium dioxide particles in the absence of photoactivation can induce oxidative damage to human bronchial epithelial cells. *Toxicology*, **213**, 66-73.

Heppleston AG (1984). Pulmonary toxicology of silica, coal and asbestos. *Environ Health Perspect*, **55**, 111-27.

IARC (2010). Carbon black, titanium dioxide, and talc. *IARC Monogr Eval Carcinog Risks Hum*, **93**, 1-413.

Kakinoki K, Yamane K, Teraoka R, et al (2004). Effect of relative humidity on the photocatalytic activity of titanium dioxide and photostability of famotidine. *J Pharm Sci*, **93**, 582-9.

Maynard AD, Aitken RJ, Butz T, et al (2006). Safe handling of nanotechnology. *Nature*, **444**, 267-9.

Mohr U, Ernst H, Roller M, et al (2006). Pulmonary tumor types induced in Wistar rats of the so-called "19-dust study". *Exp Toxicol Pathol*, **58**, 13-20.

Nel A, Xia T, Madler L, et al (2006). Toxic potential of materials at the nanolevel. *Science*, **311**, 622-7.

Renwick LC, Donaldson K, Clouter A (2001). Impairment of alveolar macrophage phagocytosis by ultrafine particles.

Toxicol Appl Pharmacol, **172**, 119-27.

Rom WN, Travis WD, Brody AR (1991). Cellular and molecular basis of the asbestos-related diseases. *Am Rev Respir Dis*, **143**, 408-22.

Sayes CM, Wahi R, Kurian PA, et al (2006). Correlating nanoscale titania structure with toxicity: a cytotoxicity and inflammatory response study with human dermal fibroblasts and human lung epithelial cells. *Toxicol Sci*, **92**, 174-85.

Schulte P, Geraci C, Zumwalde R, et al (2008). Occupational risk management of engineered nanoparticles. *J Occup Environ Hyg*, **5**, 239-49.

Tsuda H, Xu J, Sakai Y, Futakuchi M, Fukamachi K (2009). Toxicology of engineered nanomaterials - A review of carcinogenic potential. *Asian Pac J Cancer Prev*, **10**, 975-980.

Wang H, Li J, Quan X, et al (2007). Formation of hydrogen peroxide and degradation of phenol in synergistic system of pulsed corona discharge combined with TiO_2 photocatalysis. *J Hazard Mater*, **141**, 336-43.

Wu J, Liu W, Xue C, et al (2009). Toxicity and penetration of TiO_2 nanoparticles in hairless mice and porcine skin after subchronic dermal exposure. *Toxicol Lett*, **191**, 1-8.

Xu J, Futakuchi M, Iigo M, et al (2010). Involvement of macrophage inflammatory protein 1alpha (MIP1alpha) in promotion of rat lung and mammary carcinogenic activity of nanoscale titanium dioxide particles administered by intrapulmonary spraying. *Carcinogenesis*, **31**, 927-35.

Arch Toxicol
DOI 10.1007/s00204-013-1086-5

INORGANIC COMPOUNDS

Nanosized zinc oxide particles do not promote DHPN-induced lung carcinogenesis but cause reversible epithelial hyperplasia of terminal bronchioles

Jiegou Xu · Mitsuru Futakuchi · David B. Alexander · Katsumi Fukamachi · Takamasa Numano · Masumi Suzui · Hideo Shimizu · Toyonori Omori · Jun Kanno · Akihiko Hirose · Hiroyuki Tsuda

Received: 25 February 2013 / Accepted: 20 June 2013

Abstract Zinc oxide (ZnO) is known to induce lung toxicity, including terminal bronchiolar epithelial hyperplasia, which gives rise to concerns that nanosized ZnO (nZnO) might lead to lung carcinogenesis. We studied the tumor promoting activity of nZnO by an initiation–promotion protocol using human c-Ha-*ras* proto-oncogene transgenic rats (H*ras*128 rats). The rats were given 0.2 % N-nitrosobis(2-hydroxypropyl)amine (DHPN) in the drinking water for 2 weeks and then treated with 0.5 ml of 250 or 500 μg/ml nZnO suspension by intra-pulmonary spraying once every 2 weeks for a total of 7 times. Treatment with nZnO particles did not promote DHPN-induced lung carcinogenesis. However, nZnO dose-dependently caused epithelial hyperplasia of terminal bronchioles (EHTB) and fibrosis-associated interstitial pneumonitis (FAIP) that were independent of DHPN treatment. Tracing the fate of EHTB lesions in wild-type rats indicated that the hyperplastic lesions almost completely disappeared within 12 weeks after the last nZnO treatment. Since nZnO particles were not found in the lung and $ZnCl_2$ solution induced similar lung lesions and gene expression profiles, the observed lesions were most likely caused by dissolved Zn^{2+}. In summary, nZnO did not promote carcinogenesis in the lung and induced EHTB and FAIP lesions that regressed rapidly, probably due to clearance of surplus Zn^{2+} from the lung.

Keywords Nanosized zinc oxide particles · Lung toxicity · Lung carcinogenesis · Epithelial hyperplasia of terminal bronchioles · Interstitial pneumonitis · Lung fibrosis

Electronic supplementary material The online version of this article (doi:10.1007/s00204-013-1086-5) contains supplementary material, which is available to authorized users.

J. Xu · D. B. Alexander · H. Tsuda (✉)
Laboratory of Nanotoxicology Project, Nagoya City University, 3-1 Tanabedohri Mizuho-ku, Nagoya 467-8603, Japan
e-mail: htsuda@phar.nagoya-cu.ac.jp

J. Xu · M. Futakuchi · K. Fukamachi · T. Numano · M. Suzui
Department of Molecular Toxicology, Nagoya City University Graduate School of Medical Sciences, 1-Kawasumi, Mizuho-cho, Mizuho-ku, Nagoya 467-8601, Japan

H. Shimizu
Core Laboratory, Nagoya City University Graduate School of Medical Sciences, 1-Kawasumi, Mizuho-cho, Mizuho-ku, Nagoya 467-8601, Japan

T. Omori
Department of Health Care Policy and Management, Nagoya City University Graduate School of Medical Sciences, 1-Kawasumi, Mizuho-cho, Mizuho-ku, Nagoya 467-8601, Japan

J. Kanno · A. Hirose
National Institute of Health Sciences, 1-18-1 Kamiyoga, Setagaya-ku, Tokyo 158-8501, Japan

Introduction

One of the most widely used nanomaterials is nZnO. The worldwide production of nZnO powder is increasing every year and was reported to have reached 1.4 million tons in 2011. It is used in rubber industry and electronics and in commercial products such as sunscreens and paints. In the biomedical field, it is used in baby powders, antiseptic ointments, and zinc oxide tapes to treat a variety of skin conditions (Baldwin et al. 2001; Hughes and McLean 1988). Recently, nZnO has gained interest in cancer applications or as an active anticancer drug (Rasmussen et al. 2010).

Micron or larger-sized ZnO particles are considered to be "Generally Recognized as Safe" (GRAS) in food

Published online: 06 July 2013

additives by the FDA. However, exposure to fumes containing ZnO and other metal particles during welding or galvanizing processes is known to lead to metal fume fever (Antonini et al. 2003; Drinker and Fairhall 1933; Fine et al. 1997). Recent reports have shown that nZnO affects cell viability and induces reactive oxygen species (ROS) in many mammary cell types in tissue culture (Deng et al. 2009; Lee et al. 2008; Xia et al. 2008; Yang et al. 2009), cause proliferation of airway epithelial cells, goblet cell hyperplasia, interstitial pulmonary inflammation and fibrosis (Cho et al. 2011), and reversible inflammatory reaction in the bronchoalveolar lavage fluid in animal studies (Sayes et al. 2007; Warheit et al. 2009). nZnO also leads to DNA damage (Kermanizadeh et al. 2012) and micronuclei formation in vitro (Valdiglesias et al. 2013). While these in vitro and in vivo studies have provided some information on acute toxic effects of nZnO on certain cell types and animals, further in vivo studies are needed to determine whether nZnO has chronic toxic effects as in some other metal oxide particles. For example, epidemiological data indicate that exposures of aluminum oxide or iron oxide lead to pneumoconiosis in human (Hull and Abraham 2002; Sano 1963); titanium dioxide has carcinogenic activity in the rat lung (Heinrich et al. 1995; Xu et al. 2010). Such chronic toxicity data will have more impact on risk assessment of nZnO.

Since nZnO induces inflammatory reaction, ROS production, and genotoxicity, which are implicated in cancer development, in the present study, we tested the lung carcinogenicity of nZnO by an initiation–promotion protocol using human c-Ha-*ras* proto-oncogene transgenic (H*ras* 128) rats, which have the same susceptibility to chemically induced lung carcinogenesis as their parent wild-type rats, but are highly susceptible to mammary tumor induction (Tsuda et al. 2005). The results indicated that nZnO did not have promotion effect on DHPN-induced lung and mammary carcinogenesis and caused reversible EHTB and FAIP.

Materials and methods

Animals

Forty-three female transgenic rats carrying the human c-Ha-RAS proto-oncogene (H*ras*128 rats) and 42 female wild-type Sprague–Dawley rats were obtained from CLEA Japan Co., Ltd. (Tokyo, Japan). The animals were housed in the Animal Center of Nagoya City University Medical School and maintained on a 12-h light/12-h dark cycle and received Oriental MF basal diet (Oriental Yeast Co. Ltd., Tokyo, Japan) and water ad libitum. The study was conducted according to the Guidelines for the Care and Use of Laboratory Animals of Nagoya City University Medical School, and the experimental protocol was approved by the Institutional Animal Care and Use Committee (H22M-19).

Preparation, characterization of nZnO suspensions, and administration of nZnO to the lung

Zinc oxide particles (CAS No. 1314-13-2, MZ-500, without coating, with a mean primary diameter of 25 nm) were obtained from Tayca Cooperation, Osaka, Japan. The particles were suspended in 0.1 % Tween 20 saline at 250 or 500 μg/ml. The suspension was sonicated for 20 min to prevent aggregate formation.

Characterization of nZnO was conducted as follows: the shape of nZnO in the suspensions was imaged by transmission electron microscopy (TEM); element analysis was performed by an X-ray microanalyzer (EDAX, Tokyo, Japan), after aliquots of nZnO were loaded on a carbon sheet; the size distribution of nZnO in the 500 μg/ml suspension was analyzed using a Particle Size Distribution Analyzer (Shimadzu Techno-Research, Inc., Kyoto, Japan). The characterization results are shown in Figure S1.

Before being administrated to rats, the nZnO suspensions were further sonicated for 20 min. 0.5 ml of the nZnO suspensions was administrated to the lung by intra-pulmonary spraying (IPS) as described previously (Xu et al. 2010).

Carcinogenicity study

The carcinogenic activity of nZnO was assessed in female H*ras*128 rats using an initiation–promotion protocol by which we used previously to evaluate lung and mammary carcinogenicity of titanium dioxide nanoparticles (Xu et al. 2010). Briefly, three groups of 10–11 female H*ras*128 rats aged 6 weeks were given 0.2 % DHPN (Wako Chemicals, Co., Ltd. Osaka, Japan) in the drinking water for 2 weeks, and Groups 4 and 5 (6 rats each) were given drinking water without DHPN. Two weeks later, Group 1 and Group 4 were administered 0.1 % Tween 20 saline, and Group 2, Group 3, and Group 5 were administered 250, 500, and 500 μg/ml nZnO suspensions by IPS once every two weeks from the end of week 4 to week 16, a total of 7 times. The total amounts of nZnO administered to Groups 1, 2, 3, 4, and 5 were 0, 0.875, 1.75, 0, and 1.75 mg/rat, respectively. The dosing was determined according to the permissible exposure limit for zinc oxide particles of the Occupational Safety and Health Administration (OSHA) (see Discussion). Three days after the last treatment, animals were killed and the organs (brain, lung, liver, spleen, kidney, mammary gland, ovaries, uterus, and neck lymph nodes) were fixed in 4 % paraformaldehyde in PBS buffer adjusted to pH 7.3 and processed for histological examination and transmission electron microscopy (TEM).

Light microscopy, polarized light microscopy, and transmission electron microscopy

Hematoxylin–Eosin (H&E)-stained pathological slides of the lung and other major organs were used to observe nZnO with a light microscope and polarized light microscope (PLM) (Olympus BX51N-31P-O polarized light microscope, Tokyo, Japan) at 1,000× magnification. Localization of the illuminated particles was confirmed in the same H&E-stained sections after removing the polarizing filter.

Paraffin blocks were deparaffinized and embedded in epon resin and processed for nZnO observation and zinc element analysis, using a JEM-1010 transmission electron microscope (TEM) (JEOL, Co. Ltd, Tokyo, Japan) equipped with an X-ray microanalyzer (EDAX, Tokyo, Japan).

Immunohistochemistry and Azan–Mallory staining

PCNA was detected using an anti-PCNA monoclonal antibody (Clone PC10, Dako Japan Inc., Tokyo, Japan). The antibody was diluted 1:200 in blocking solution and applied to deparaffinized slides, and the slides were incubated at 4 °C overnight. The slides were then incubated for 1 h with biotinylated species-specific secondary antibodies diluted 1:500 (Vector Laboratories, Burlingame, CA) and visualized using avidin-conjugated horseradish peroxidase complex (ABC kit, Vector Laboratories). To assess lung fibrosis, paraffin-embedded slides were deparaffinized, and collagen fibers were visualized by Azan–Mallory staining.

Reversibility study and effects of $ZnCl_2$ solution

To assess whether nZnO-induced terminal bronchiolar epithelial hyperplasia, interstitial pneumonitis, and lung fibrosis are reversible, we conducted reversibility experiments. Seven groups of 5 female wild-type Sprague–Dawley rats aged 10 weeks were administrated 0.5 ml of 0.1 % Tween 20 saline or 500 μg/ml nZnO suspension by IPS 2 times per week for 4 weeks. Group 1 was treated with 0.1 % Tween 20 saline and killed 1 day after the last IPS. Groups 2–7 were treated with 0.5 ml of 500 μg/ml nZnO suspension and killed at 1 day and 2, 4, 6, 8, and 12 weeks after the last IPS. For the comparison of the effects of zinc ion and nZnO, Group 8 was treated with 0.5 ml of 6.17 mM $ZnCl_2$ solution (the molecular amount is equal to that of 500 μg/ml nZnO suspension) by IPS at the same frequency and time period as the nZnO groups and killed 1 day after the last IPS. The left lung was cut into pieces and frozen in liquid nitrogen for biochemical analysis, and the right lung was processed for histological examination. Other major organs were excised for histological examination, and the blood was collected for cytological and biochemical analysis.

Gene expression analysis

The left lungs from Groups 1, 2, and 8 in the reversibility study described above were used for isolation of RNA. RNA was isolated by using TRizol reagent (Invitrogen of Life Technologies, CA).

For microarray analysis, 1 μg RNA from each rat of Group 1 was combined and 1 μg RNA from each rat of Group 2 was combined. The quality of the 2 mixtures of RNA samples was assessed and quantified using the Agilent 2100 BioAnalyzer RNA Nano chip system (Agilent Technologies, CA) prior to further manipulation. Microarray analysis was conducted by the 3-D Gene Chip (Toray Industries Inc., Kanagawa, Japan), and a total of 20,000 genes were analyzed. Microarray-based pathway analysis was performed by Toray Industries Inc., Kanagawa, Japan.

For reverse transcription-PCR (RT-PCR) and real-time PCR, first-strand cDNA synthesis from 1 μg of RNA was performed using SuperScript™ III First-Strand Synthesis System (Invitrogen of Life Technologies, CA) according to the manufacturer's instructions. Primers are as follows: forward primer, 5′-TAGAATCGAGGTGCACAGGAGT-3′, reverse primer, 5′-TATTCCAGCAGGCTGTCAAAGA-3′, product size, 228 bp for Orm1; forward primer, 5′-AAGTGGAGGAGCAGCTGGAGTGG-3′, reverse primer, 5′-CCAAAGTAGACCTGCCCGGACTC-3′, product size, 155 bp for Tnfa, and forward primer, 5′-AGCCATGTACGTAGCCATCC-3′, reverse primer, 5′-CTCTCAGCTGTGGTGGTGAA-3′, product size, 228 bp for Actb. RT-PCR was conducted using an iCycler (BioRad Life Sciences, CA) as follows: 95 °C 20 s, 60 °C 20 s, 72 °C 30 s, 30 cycles for Orm1; 95 °C 20 s, 60 °C 20 s, 72 °C 20 s, 25 cycles for Tnfa, and 95 °C 20 s, 60 °C 20 s, 72 °C 30 s, 15 cycles for Actb. Real-time PCR analysis of Orm1 and Tnfa gene expression was performed with the 7300 real-time PCR system (Applied Biosystem, CA) using the premix reagent Power SYBR Green PCR Master Mix (Applied Biosystem, CA) according to the manufacturer's instructions. The Actb gene was used as the normalizing reference gene.

Determination of zinc ion

For detection of Zn^{2+} content in the lung tissue, 50–100 mg of the frozen lung tissues from the reversibility study described above were thawed at room temperature, rinsed with cold PBS 3 times, and homogenized for 30 s at the highest speed in 1 ml of T-PER, tissue protein extraction reagent (Pierce, Rockford, IL), with Polytron R PT 2100 homogenizer (Capitol Scientific Inc., TX). The homogenates were clarified by centrifugation at 10,000×g for 15 min at 4 °C, and the supernatants were used for Zn^{2+}

detection. Zn^{2+} detection was performed using QuantiChrom™ Zinc Assay kit (BioAssay Systems, CA) according to the manufacturer's instructions.

In vitro nZnO dissolution assay

5 μl of 500 μg/ml nZnO suspension (2.5 μg/tube) and increasing amounts of 1 mg/ml human α 1 acid glycoprotein (Sigma-Aldrich, product number G9885) or bovine serum albumin (Sigma-Aldrich, product number A2058) were added to microtubes, and the total volume of each tube was adjusted to 100 μl with 0.1 % Tween 20 saline. The final protein concentration of human α 1 acid glycoprotein or bovine serum albumin was 0, 100, 200, 300, 400, and 500 μg/ml. The tubes were then incubated at 37 °C for 2 h. The nZnO particles were removed by centrifugation at 10,000×*g* for 5 min, and Zn^{2+} concentration in the supernatants was determined as described above.

In vitro cytotoxicity assay

The induction and preparation of rat primary alveolar macrophages (PAM) has been described (Xu et al. 2010). 5×10^3 PAMs, 1×10^3 A549 cells (human lung adenocarcinoma cell line), and 2×10^3 CCD34 cells (human lung fibroblast cell line) were seeded into 96-well culture plates and cultured overnight in 100 ml of RPMI 1,640 containing 10 % FBS. The cells were added with nZnO suspension or ZnCl2 solution to final concentrations of 0, 1, 5, or 25 μg/ml of nZnO and 0, 12.3, 61.7, or 308.6 nM of ZnCl2 (1, 5, and 25 μg/ml of nZnO are equal to 12.3, 61.7, and 308.6 nM of ZnCl2, respectively, in the amount of zinc element) and incubated for another 72 h. The cell viability was then determined using the Cell Counting Kit-8 (Dojindo Molecular Technologies, Rockville, MD) according to the manufacturer's instruction.

Statistical analysis

Statistical analysis was performed using ANOVA. Statistical significance was analyzed using a two-tailed Student's *t*-test. A p value of <0.05 was considered to be significant.

Results

Carcinogenesis study in H*ras*128 rats

DHPN-induced lung alveolar cell hyperplasia and adenoma development was used for the end point observation to assess the carcinogenicity of nZnO in our medium-term assay. As shown in Table 1, the incidence and multiplicity (number/cm^2 lung tissue section) of

Table 1 Effect of nZnO on lung proliferative lesions in H128-*ras* rats

Treatment	No. of rats	DHPN-induced proliferative lesions						DHPN-independent EHTB[a]	
		ACH[a]		Ade[a]		ACH + Ade		Inc. (%)	Multiplicity[b] (no./cm^2 lung)
		Inc.[a] (%)	Multiplicity[b] (no./cm^2 lung)	Inc. (%)	Multiplicity[b] (no./cm^2 lung)	Inc. (%)	Multiplicity[b] (no./cm^2 lung)		
DHPN + vehicle	11	11 (100)	2.43 ± 1.29	2 (18.1)	0.09 ± 0.20	11 (100)	2.52 ± 1.26	0 (0)	0
DHPN + 250 μg/ml nZnO	10	10 (100)	1.64 ± 1.09	3 (30.0)	0.12 ± 0.19	10 (100)	1.76 ± 1.03	7 (70)	0.86 ± 0.86 **
DHPN + 500 μg/ml nZnO	10	10 (100)	1.83 ± 1.05	5 (50.0)	0.30 ± 0.31	10 (100)	2.13 ± 1.23	10 (100)	4.93 ± 1.95 ***
Vehicle	6	0	0	0	0	0	0	0	0
500 μg/ml nZnO	6	2 (33.3)	0.16 ± 0.26	0	0	2 (33.3)	0.16 ± 0.26	6 (100)	3.91 ± 1.29 ***

[a] ACH, Ade, EHTB, and Inc. are abbreviations for alveolar cell hyperplasia, adenoma, epithelial hyperplasia of terminal bronchioles, and incidence, respectively

[b] Multiplicity is expressed as mean ± s.d

** and *** represent p values <0.01 and 0.001, respectively, versus DHPN + vehicle or vehicle

alveolar cell hyperplasia and adenoma in the groups treated with nZnO were not significantly different from the DHPN alone group. In the rats which received nZnO treatment without prior DHPN treatment, alveolar cell proliferation foci, recognized as thickening of the alveolar wall with proliferative alveolar epithelium, were observed, but significant differences from the saline group were not observed. In the mammary gland, significant inter-group difference in incidence and multiplicity of mammary tumors was also not observed (data not shown).

A notable lesion induced in all the nZnO-treated groups was epithelial hyperplasia of terminal bronchioles (EHTB). The EHTB lesions had increased cell density, often with the epithelial cells arranged in 1–3 layers, and partly extended bronchiolar structures with transition to the normal

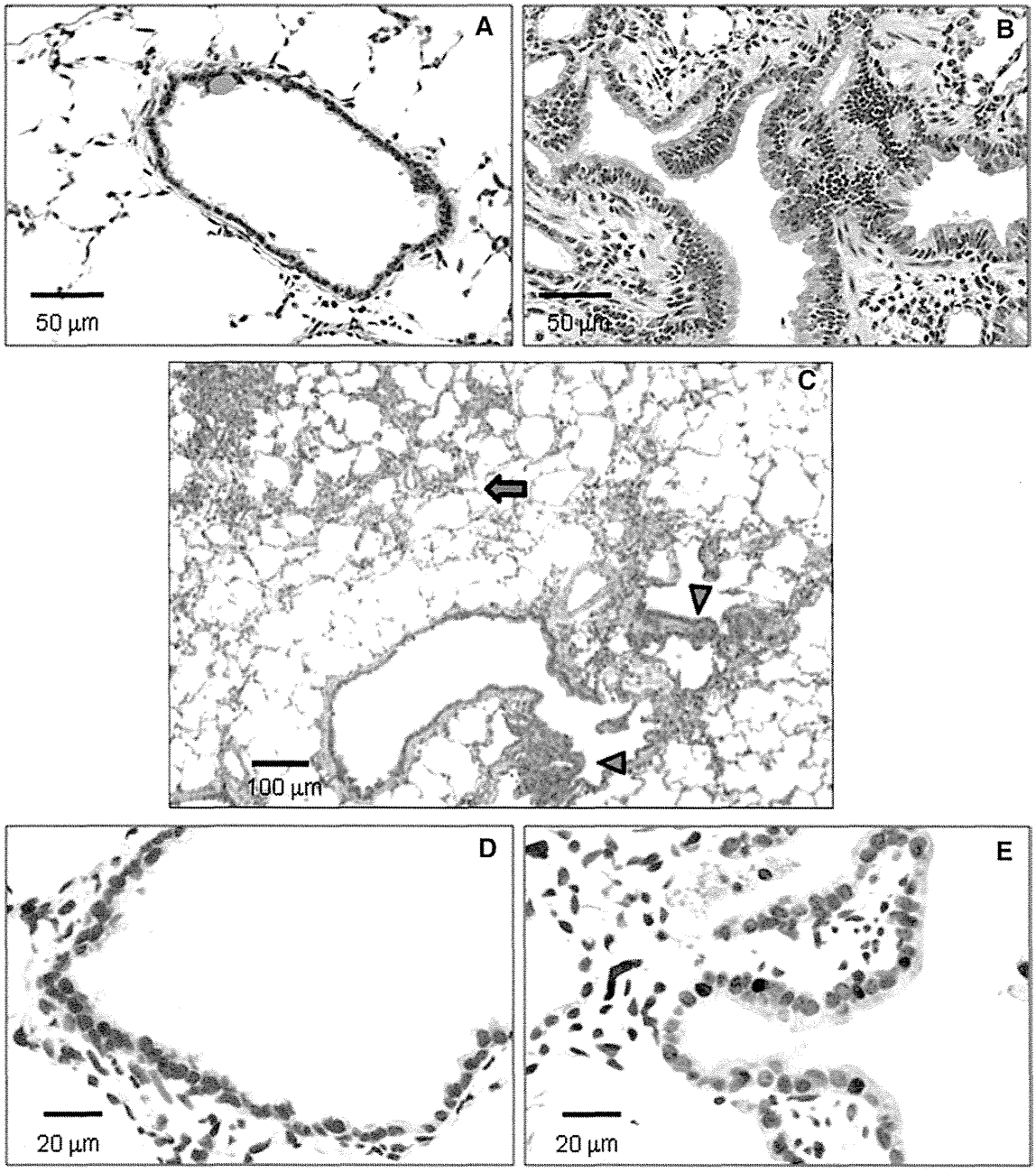

Fig. 1 Induction of EHTB by nZnO. **a** representative normal terminal bronchiolar epithelium (NTBE); **b** EHTB in H&E-stained slides; **c** images and localizations of DHPN-induced alveolar hyperplasia (*arrow*) and nZnO-induced EHTB (*arrow heads*); **d** images of PCNA immunostaining in NTBE; and **e** in EHTB

terminal bronchioles (Fig. 1a, b). The EHTB lesions were independently localized from the DHPN-induced alveolar cell hyperplastic lesions (Fig. 1c). The incidences and multiplicity (number/cm^2 lung tissue section) of EHTB in the groups treated with nZnO were significantly increased compared with that of the DHPN alone group. The increase was dose-dependent (Spearman rank correlation test, $p < 0.001$) (Table 1). Immunostaining with proliferating cell nuclear antigen (PCNA) indicated that proliferating bronchiolar epithelial cells were preferentially found in the EHTB lesions, but rarely found in the normal terminal bronchial epithelial areas (Fig. 1d, e).

Another lesion found in the groups treated with nZnO, and also independent of DHPN treatment, was interstitial pneumonitis (Fig. 2a). The lesion was usually associated with fibrosis of various thicknesses of the septal wall extruding into the alveolar structure (blue staining in Fig. 2b). Quantitative analysis indicated a significant increase in the fibrotic area in the rats treated with nZnO compared with that of rats treated with DHPN alone (Fig. 2c), and the increase was dose-dependent (Spearman rank correlation test, $p < 0.001$). In addition, the EHTB lesions often occurred near or within interstitial pneumonitis areas.

Light microscopic observation of the alveoli of the rats treated with nZnO showed infiltration of numerous macrophages mixed with a few neutrophils, eosinophils, and lymphocytes (data not shown). The nZnO particles were not found in any of the alveolar macrophages; these macrophages contained numerous vacuolar vesicles in the cytoplasm (Fig. 2d). Transmission electron microscopic (TEM) observation showed that nZnO particles were not found within the vacuolar vesicles (Fig. 2e) or in any alveolar tissue cells (Fig. 2f). The absence of a zinc peak was confirmed by elemental scanning with TEM-X-ray microanalysis (Figure S2). nZnO particles were also not detected under polarized light microscope observation. This feature was in contrast with titanium dioxide nanoparticles which were clearly observed in alveolar macrophages (Figure S3).

Reversibility of EHTB and FAIP in wild-type rats

As in the H*ras*128 transgenic rats, nZnO induced EHTB and FAIP in wild-type Sprague–Dawley (SD) rats (Fig. 3a), and nZnO was not found in the lung tissue. nZnO-induced EHTB and FAIP gradually regressed with time (Fig. 3a), and the number of EHTB foci per square centimeter lung tissue section decreased from 9.81 ± 1.42 at day 1 to 0.06 ± 0.13 at week 12 after cessation of nZnO exposure (Fig. 3b). The total Zn^{2+} content in the lung tissue also gradually decreased (Fig. 3c) and was positively correlated with the number of EHTB ($r = 0.96$ by Pearson correlation test).

Microarray analysis

Microarray analysis of the lung tissue indicated that nZnO treatment up-regulated the expression of 738 genes and down-regulated the expression of 267 genes (data not shown). The up-regulated inflammation-associated genes included chemotactic chemokines such as Cxcl5, Cxcl11, Ccl7, Cxcl2, Ccl2, and Cxcl1, proinflammatory cytokines such as Tnfa and Il6, and the acute-phase reactant Orm1 (Table S1). Pathway analysis showed an increase in inflammatory responses in which macrophages and TNFα play a central role (Figure S4). The gene expression profiling was consistent with the strong inflammatory responses in the lung observed by histological examination. Other pathways up-regulated by nZnO included classical complement activation pathway, matrix metalloproteinase pathway, cholesterol biosynthesis pathway and striated muscle contraction pathway, and treatment of nZnO down-regulated the adipogenesis pathway (data not shown).

Effects of $ZnCl_2$ solution on the lung of wild-type rats

To check whether the nZnO-induced EHTB and FAIP were due to dissolution of nZnO to Zn^{2+}, we administered $ZnCl_2$ solution (the molecular amount is equal to that of 500 μg/ml nZnO suspension) to the lung of rats by IPS. The lesions were histologically similar to those observed in the nZnO-treated rats (Fig. 4a, b, c). Quantitative analysis of EHTB indicated that the number of EHTB induced by $ZnCl_2$ solution and nZnO was comparable (Fig. 4d).

To examine whether Zn^{2+} and nZnO have the same underlying molecular mechanisms, two genes, Tnfa and Orm1, which were determined to be up-regulated in the nZnO-treated rats by microarray analysis, were chosen for gene expression analysis. These genes were chosen because Tnfa-encoded tumor necrosis factor alpha is a multifunctional proinflammatory cytokine involved in a variety of acute and chronic inflammatory responses, and Orm1-encoded alpha 1 acid glycoprotein (AGP) is an acute-phase protein usually synthesized by hepatocytes in response to trauma, infection, and inflammation (Fournier et al. 2000). RT-PCR (Fig. 4e) and real-time PCR (Fig. 4f) showed that treatment with both $ZnCl_2$ solution and nZnO increased the expression of Tnfa and Orm1 genes in the lung tissue, with a little higher induction in the $ZnCl_2$ solution treated rats. Similarly, increased expression of Orm1 genes was found in primary alveolar macrophages exposed to nZnO in vitro (Fig. 4g). Interestingly, addition of human AGP to nZnO suspension dose-dependently promoted dissolution of nZnO from 59.1 nmol/ml (19.7 % dissolved,

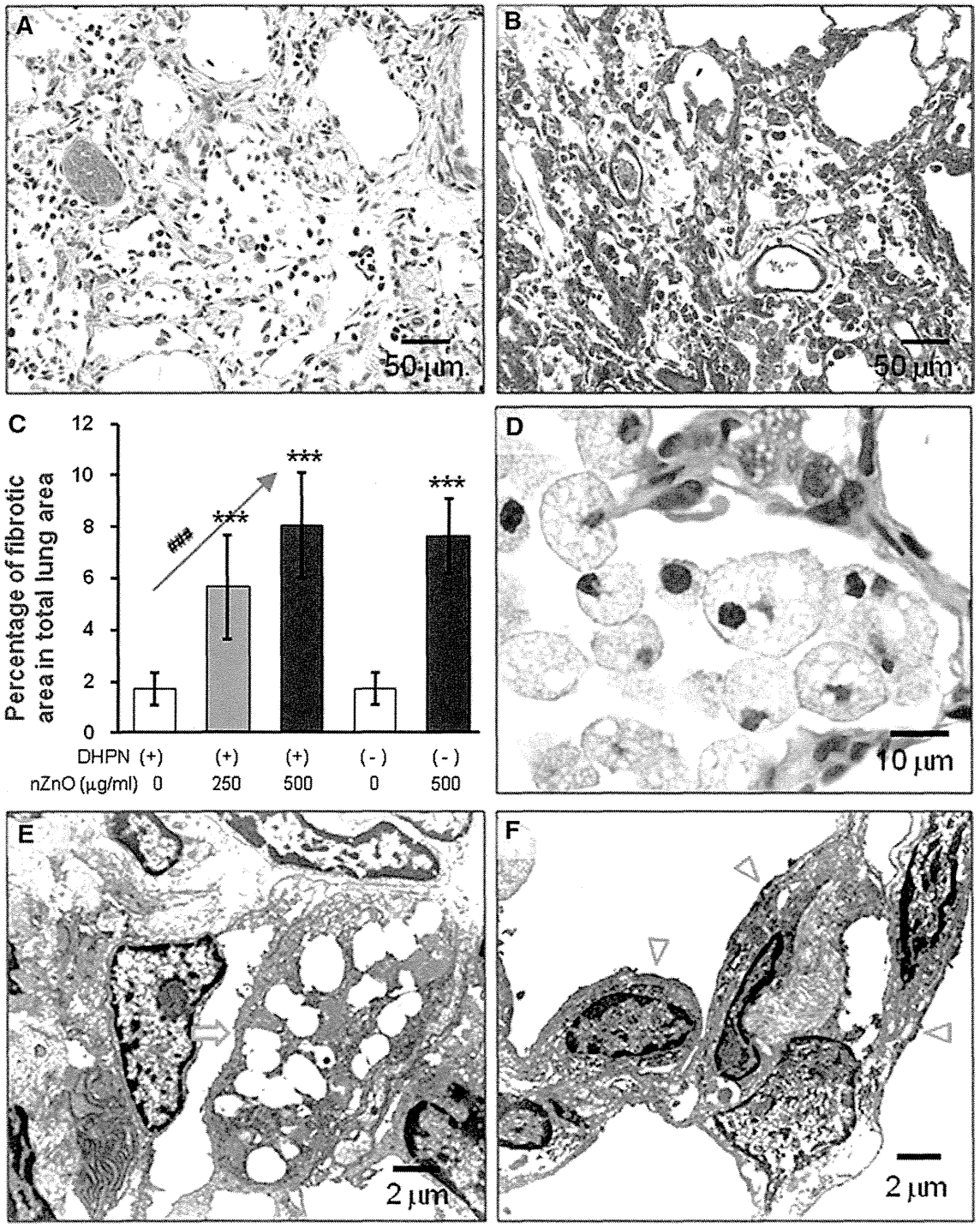

Fig. 2 Induction of FAIP and observation of nZnO particles. **a** representative image of FAIP in rats treated with nZnO; **b** image of Azan–Mallory staining in the lung of rats treated with nZnO, showing collagen fibers; **c** percentage of the fibrotic area in total lung tissue area. ***<0.001 by two-tailed Student's *t*-test versus the vehicle group; and ###$p < 0.001$ by Spearman rank correlation test. **d** image showing alveolar macrophages with vacuous phagocytosis vesicles; **e** and **f** TEM images showing alveolar macrophages (*arrow*) and epithelium (*arrow heads*), no nZnO particles being observed

without addition of AGP) to 117.3 nmol/ml (39.1 % dissolved after addition of 500 μg/ml of AGP), while addition of bovine serum albumin (BSA) had little effect on dissolution of nZnO (Fig. 4h). Exposure of both nZnO and $ZnCl_2$ solution resulted in dose-dependent cell death in vitro (Figure S5).

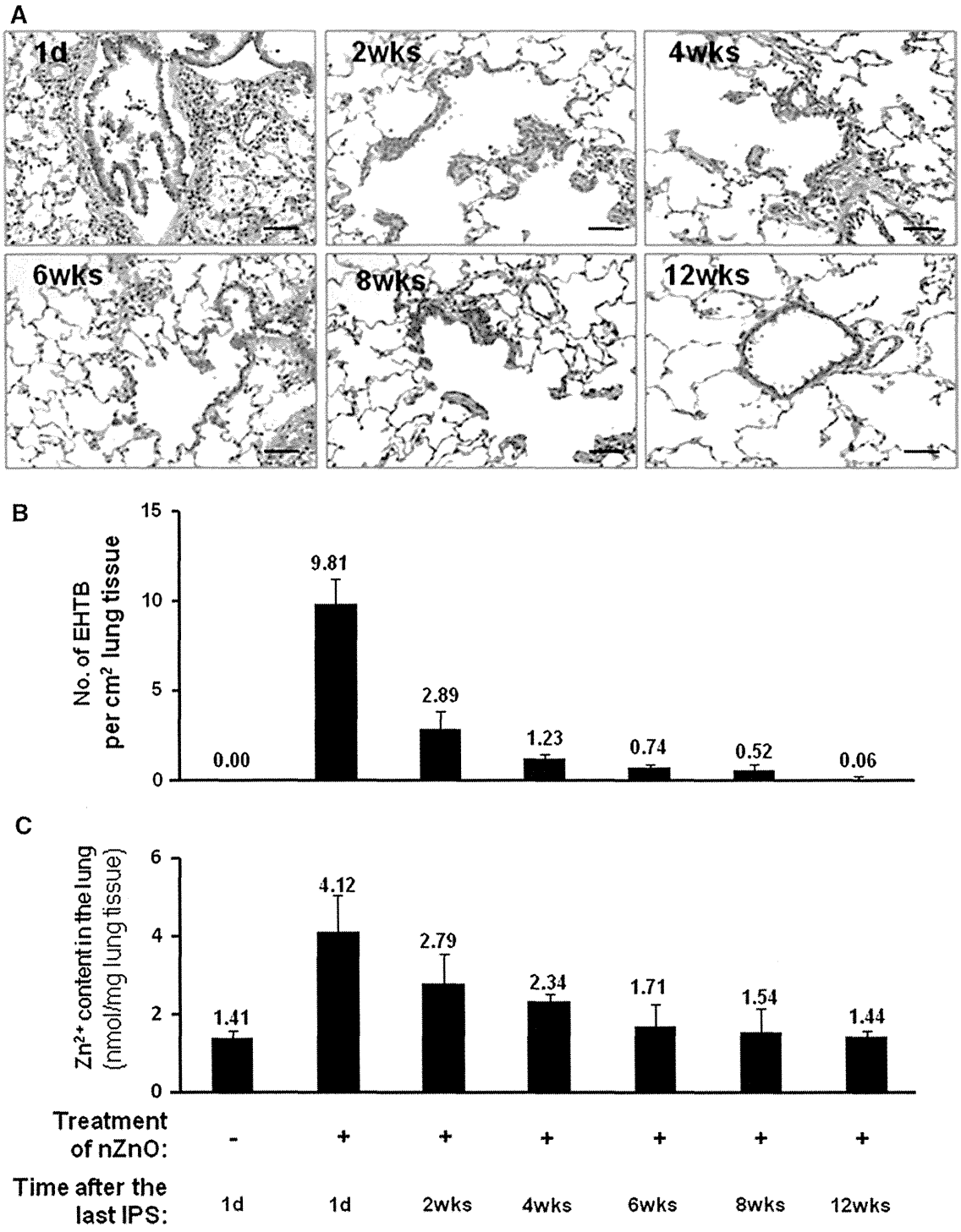

Fig. 3 nZnO-induced EHTB and FAIP are reversible. Wild-type rats were treated with 500 μg/ml nZnO by IPS 2 times/week for 4 weeks and killed at different time points of 1 day (1d) and 2, 4, 6, 8, and 12 weeks (wks) after the last IPS. **a** histological images of the lung tissues; **b** number of EHTB per cm^2 lung tissue and **c** Zn^{2+} content in the lung tissues at different time points. *Bars* = 50 μm

Effects of nZnO particles and $ZnCl_2$ solution on other organs and serum of wild-type rats

Obvious lesions and macrophages containing vacuolar vesicles were not found in other major organs including the liver, kidney, spleen, or brain by histological examination (data not shown). The results of blood cell examination are shown in Table S2: The only changes were increased proportions of monocytes and eosinophils that were rapidly recovered within 2 weeks post exposure. Biochemical

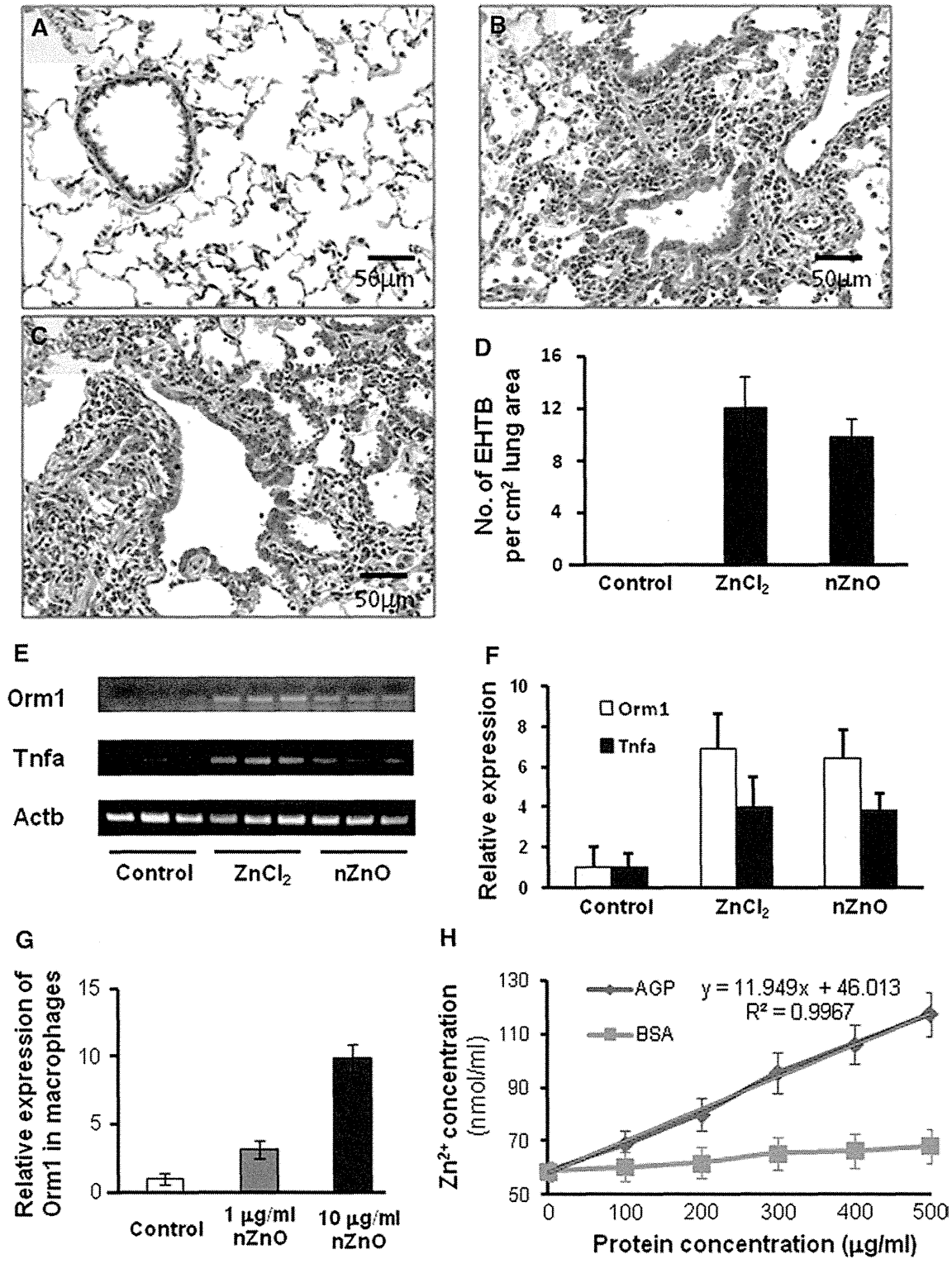

Fig. 4 Similar effects of $ZnCl_2$ solution and nZnO in induction of EHTB and FAIP in wild-type rats. **a** H&E-stained slides of the lungs of rats treated with vehicle; **b** with nZnO; and **c** with $ZnCl_2$ solution, showing EHTB and FAIP; **d** comparable number of EHTB per square centimeter of the lung tissues induced by treatment of $ZnCl_2$ and nZnO; **e** gene expression determined by RT-PCR of Orm1 and Tnfa, with Actb gene as an internal control; **f** real-time PCR analysis of gene expression of Orm1 and Tnfa, which was normalized with Actb expression; **g** induction of Orm1 expression in primary alveolar macrophages exposed to nZnO; and **h** effect of human alpha 1 acid glycoprotein (AGP) and bovine serum albumin (BSA) on dissolution of nZnO in vitro

examination of serum markers for tissue and organ injuries indicated no significant changes compared to the vehicle group (Table S3). Administration of nZnO or $ZnCl_2$ to the lung led to a transient increase in serum Zn^{2+} concentration which returned to normal levels within 2 weeks after administration. The elevated serum Zn^{2+} did not affect the homeostasis of the other ions examined (Table S4).

Discussion

In vivo nanomaterial toxicity usually implicates oxidative stress, inflammation (Nel et al. 2006), and other biological responses depending on the individual nanomaterial. In vitro assays related to carcinogenicity, such as mammalian cell transformation and gene mutation assays, cannot represent the complex in vivo processes of different biological alterations and are not always suitable for risk assessment of nanomaterial carcinogenicity. In the present study, we tested the carcinogenic activity of nZnO in H*ras*128 rats by an initiation–promotion protocol, by which we previously found promotion effect of nanosized titanium dioxide on DHPN-induced lung and mammary carcinogenesis (Xu et al. 2010). nZnO did not show any promotion effects on lung proliferative or neoplastic lesions, indicating that nZnO is not carcinogenetic. Also, nZnO did not promote DHPN-induced mammary carcinogenesis.

On the other hand, nZnO was found to induce EHTB in H*ras*128 rats and wild-type SD rats. EHTB is a proliferative lesion of the terminal bronchiolar epithelium. It should be noted that the localization of EHTB was independent from that of DHPN-induced alveolar cell hyperplasia. This observation clearly indicates that the DHPN-induced alveolar cell hyperplasia and EHTB have different etiology, the latter being induced by nZnO. We also observed 2 cases of alveolar cell hyperplasia out of 6 cases in the nZnO alone group. This is not significant and thus considered to be spontaneous or an inflammation-associated event. The EHTB lesions regressed when administration of nZnO was discontinued and completely disappeared after 12 weeks. Along with EHTB, the interstitial inflammatory changes often observed surrounding the EHTB lesions also regressed. Our data and other reports (Cho et al. 2011) indicate that the EHTB lesions do not progress directly to cancers but are reactive proliferation associated with inflammatory events. Similar reversible inflammatory changes in the bronchoalveolar lavage fluids by administration of nanoscale or fine ZnO particles via inhalation or intratracheal instillation have previously been reported (Warheit et al. 2009).

nZnO particles were not found in alveolar macrophages, in the lung tissue, or in other organs, suggesting that the particles were dissolved to Zn^{2+}. Accordingly, we conducted experiments to determine whether Zn^{2+} would induce similar lesions. $ZnCl_2$ solution induced closely similar lung lesions and gene expression profiles as nZnO, demonstrating that the observed lung lesions were caused by Zn^{2+}. This was confirmed by increased Zn^{2+} level in the lung and serum after administration of nZnO. Interestingly, treatment with nZnO up-regulated the expression of the Omrl gene in both the lung and the alveolar macrophages, and in vitro addition of Omrl-encoded AGP dose-dependently promoted nZnO dissolution. After Zn^{2+} was cleared from the lung, the EHTB and FAIP lesions disappeared, and this was evidenced by the positive correlation of EHTB number with Zn^{2+} content in the lung. Dissolution of nZnO has been reported to be particle size- and pH-dependent (Mudunkotuwa et al. 2012). Increased Omrl expression possibly alters the microenvironment of the alveolar macrophages and the lung which accelerates nZnO dissolution. The elevated Zn^{2+} from nZnO dissolution possibly interferes with zinc ion homeostasis and leads to cytotoxic effects (Kao et al. 2012).

According to OSHA, the permissible exposure limit for zinc oxide particles is 15 mg/m^3 of air for total dust and 5 mg/m^3 for the respirable fraction (http://www.osha.gov/SLTC/healthguidelines/zincoxide/recognition.html). The inhalation exposure limit per kilogram of body weight per day for the respirable fraction is 192 μg, calculated from 6,000 ml of minute respiratory volume and 8 working hours for a 75 kg body weight worker. The dosing in the carcinogenesis study of the present study was approximately 35.5 and 71 μg/kg body weight a day (calculated from 125 to 250 μg every two weeks for a 250 g rat) and is lower than the OSHA limit for humans. Since nZnO has more potential to be ionized than larger ZnO particles because of its higher surface area (Mudunkotuwa et al. 2012), this feature should be taken into regulatory consideration.

It has been estimated that engineered nanomaterials will become a $1 trillion enterprise by 2015 (Nel et al. 2006), and ensuring health and environmental safety is a challenging task to the nanotechnology industry. Among numerous engineered nanomaterials, metal based or carbon based, most of which have been shown to have toxic effects to at least some extent, nZnO is a promising nanomaterial for biomedical applications. The results of the present study indicate that, although nZnO induced reversible lung toxicity, it did not cause carcinogenic or chronic progressive inflammatory lesions. Also, since it is biodegradable to ions, nZnO is easily cleared from the body (Rasmussen et al. 2010). Our study also suggests that the toxic effects of nZnO can be further decreased if efforts such as proper dosing and surface coating are made to lower the Zn^{2+} release from nZnO.